

Supporting Information

A Vacancy-Engineering Ferroelectric Nanomedicine for Cuproptosis/Apoptosis Co-Activated Immunotherapy

Yaqian Du, Xudong Zhao, Fei He, Haijiang Gong, Jiani Yang, Linzhi Wu, Xianchang Cui, Shili Gai, Piaoping Yang,* and Jun Lin**

Experimental Section

Chemicals: 3,3',5,5'-Tetramethylbenzidine (TMB), and methylene blue (MB) were purchased from Aladdin (Shanghai, China). 7-dichlorofluorescein diacetate (DCFH-DA), glutathione (GSH), and JC-1 staining kit, were purchased from Beyotime Institute Biotech (Haimen, China). The CCK-8 was procured from New Cell & Molecular Biotech. Calcein-AM/propidium iodide (PI) double staining, DiO cell membrane green fluorescent, ROS, mitochondrial dark red fluorescent, and JC-1 mitochondrial membrane potential assay kits were purchased from Yaseen Biotechnology Co., Ltd (Shanghai, China). Anti-CD3e-PerCP/Cyanine5.5, anti-CD4-FITC, anti-CD8a-PE, anti-CD11c-FITC, anti-CD86-APC, anti-CD80-PerCP/Cyanine5.5, anti-CD11b-APC, anti-F4/80-PerCP/Cyanine5.5 and anti-CD206-PE were obtained from Biosynthesis Biotechnology Inc. (Beijing, China). Anti-HMGB1 antibody was obtained from Biosynthesis Biotechnology Inc. (Beijing, China). FITC-goat anti-rabbit IgG(H+L) (BF05002) was obtained from Biodragon. MTT, 5,5-dimethyl-1-pyrroline N-oxide (DMPO), 4',6-diamidino-2-phenylindole (DAPI), calcein-AM, and PI were procured from Beyotime (Shanghai, China). The mouse TNF- α and IFN- γ ELISA kits were obtained from Beijing Solarbio Science & Technology Co., Ltd. (Beijing, China). Cell Freezing Medium was procured from Shanghai Chuanqiu Biotechnology Co.,Ltd, China. One Step TUNEL Apoptosis Assay Kit was procured from Beijing Solarbio Science & Technology Co., Ltd. (Beijing, China). Anti-Foxp3 (Catalog# ET1702-12, [JF0898]) was purchased from HUABIO. Anti-Bcl-2 and Anti-Bax were purchased from Shenyang Wanlei Biotechnology Co., Ltd. All chemical reagents were used without further purification.

Characterization: The morphology was visualized through TEM images acquired using a FEI Tecnai T20 transmission electron microscope. X-ray photoelectron spectroscopy (XPS) spectra was determined by an ESCALAB 250 instrument, to analyze the valence of the Cu, Bi

and O component of BCO- V_{Cu} . The UV-vis absorbance spectra of the samples were determined by a UV-1601 spectrophotometer. The electron-spin-resonance (ESR) spectra were determined using a Bruker EMX1598 spectrometer. Confocal laser scanning microscopy (CLSM) images were obtained from Leica SP8. The Western Bolt were detected by a Mini-PROTEAN® Tetra Electrophoresis tank and polyvinylidene fluoride (PVDF) membrane (Merck, Darmstadt, Germany).

·OH Generation Ability of BCO- V_{Cu} . The comparison of (1) TMB (2 mg mL⁻¹, 100 μL) + H₂O₂ (20 mM) + BCO- V_{Cu} (1 mL, 400 μg mL⁻¹) with (2) TMB (2 mg mL⁻¹, 100 μL) + H₂O₂ (20 mM) and (3) TMB (2 mg mL⁻¹, 100 μL) indicated that BCO- V_{Cu} had the ability to generate ·OH. H₂O₂ (10, 20, 40, 80, and 160 mM) was mixed with BCO- V_{Cu} (1 mL, 600 μg mL⁻¹) and TMB (2 mg mL⁻¹, 100 μL) at pH 6.5. Absorbance was monitored using UV-vis spectrometry.

Evaluation of Superoxide Anion Radical ($\cdot O_2^-$) and Singlet Oxygen (1O_2) Generation. BCO- V_{Cu} (400 μg mL⁻¹) and DPBF (20 μg mL⁻¹) were dispersed in solution. After different times of US irradiation, the absorbance at 416 nm was recorded to quantify the production rate of $\cdot O_2^-$ and 1O_2 . And, BCO was measured under the same conditions.

Electrochemical Measurements. Electrochemical measurements on BCO and BCO- V_{Cu} were conducted using an electrochemical analyzer in 0.5 M aqueous Na₂SO₄ as an electrolyte. The instrument featured three (working, reference, and platinum) electrodes. The suspension (20 μL) prepared by mixing BCO or BCO- V_{Cu} with 1 mM ethanolic Nafion (2 mL) was deposited on a conductive surface to prepare the working electrode.

Cell Culture. CT26 cells (mouse colon cancer cells) and L929 (mouse fibroblasts) cells were cultured in a humidified incubator with 5% CO₂ at 37 °C in Roswell Park Memorial Institute (RPMI 1640) supplemented with 10% fetal bovine serum (FBS, HB-FBS-50, HAKATA, Shanghai, China) and 1% antibiotics. Confocal dishes were purchased from Zhejiang Saining Biotechnology Co., Ltd. RPMI 1640 and 100x penicillin-streptomycin solution (BC.CE-007, BioChannel) were purchased from BioChannel Biological Technology Co., Ltd.

In Vitro Cellular Uptake. CT26 cells were grown in six-well plates (5 × 10⁵ cells per well) and incubated with BCO- V_{Cu} -FITC at different time intervals in a CO₂ cell incubator. Green fluorescence images were detected by CLSM.

In Vitro Synergistic Therapeutic Efficacy. CT26 cells were grown in 96-well plates and incubated overnight. The cells were randomly divided into 6 groups and irradiated with (1) PBS, (2) BCO, (3) BCO- V_{Cu} , (4) PBS + US irradiation, (5) BCO + US irradiation, and (6) BCO- V_{Cu} + US irradiation. MTT solution (20 μL) was added to each well. Finally, dimethyl

sulfoxide (100 μ L) was added. The absorbance of control cells at $\lambda = 490$ nm was measured using an enzyme labeling method, and the viability of treated cells was determined. In order to visualize the results of the treatments, live and dead cell staining experiments were carried out. CT26 cells were cultured in 6-well plates, and after different grouping treatments as described above, they were first stained with AM, then stained with PI solution, and finally fixed with glutaraldehyde. The distribution of live and dead cells was observed with CLSM.

In vitro ROS generation. CT26 cells were implanted into six-well plates. Each well of the six-well plate was divided into different groups for processing. Different groups of CT26 cells were incubated in a CO₂ cell culture incubator at 37°C for 4 h. Each well was placed in DCFH-DA probe for 0.5 h. Green fluorescence was determined by CLSM.

Western blot assays. CT26 cells were grown in six-well plates. The cells were divided into six groups and treated with (1) PBS, (2) BCO, (3) BCO-V_{Cu}, (4) PBS + US irradiation, (5) BCO + US irradiation, and (6) BCO-V_{Cu} + US irradiation, and after treatment, the collected cells were stained with Bax, Bcl-2, FDX1, DLAT, ATP7A and ATP7B antibody.

In Vitro Immunogenic Cell Death (ICD) Effect. CT26 cells were cultured overnight in six-well plates. The six-well plates were randomly divided into the following six groups and treated accordingly, and the cells in each well were irradiated with (1) PBS, (2) BCO, (3) BCO-V_{Cu}, (4) PBS + US irradiation, (5) BCO + US irradiation, and (6) BCO-V_{Cu} + US irradiation, respectively. After another 60 min of incubation, the cells were fixed, incubated with 0.3% Triton X-100 for about 5 min, and then sealed at 25°C for 20 min. The cells were washed using PBS, stained with anti-CRT antibody for 30 min, and then stained with the corresponding secondary antibody. After DAPI staining, the cells were washed three times using PBS. The difference between the above anti-HMGB1 staining method and the anti-CRT staining method is that the cells were incubated with 0.3% Triton X-100 at 25°C for 40 min, and all images were obtained by CLSM. Changes in intracellular ATP content were further detected. After the above cells were treated in different groups, they were tested using an ATP assay kit to determine the changes in ATP content in each group after different treatments.

Animal Experiments. Female BALB/c mice were obtained from Beijing Vital River Laboratory Animal Technology Co., Ltd. (Beijing, China; 1100111084356). All animal experiments were approved by the Ethics Committee of the Second Affiliated Hospital of Harbin Medical University (Harbin, China) and performed in accordance with the Guidelines for the Care and Use of Laboratory Animals of the Drug Safety Evaluation Center of Harbin Medical University (No. SYDW 2019-82).

In Vivo Biodistribution of BCO-V_{Cu}. Subcutaneously inoculate 1 million CT26 cells into mice. Mice were randomly divided into six different time groups (1, 4, 8, 12, 24, and 48 h), and BCO-V_{Cu} were injected into the tail vein. After each group reached the corresponding circulation time, the main tissues were collected, weighed, and the concentrations in each tissue were measured using ICP-MS. For *in vivo* CT and MR imaging, BCO-V_{Cu} was injected into the tumor-bearing mice.

In Vivo DCs Stimulation. BALB/c mice were subcutaneously inoculated with CT26 cells and randomly divided into 6 groups for experiments: (1) PBS, (2) BCO, (3) BCO-V_{Cu}, (4) PBS + US irradiation, (5) BCO + US irradiation, and (6) BCO-V_{Cu} + US irradiation, with 5 mice in each group. After 8 h of tail vein injection, tumor bearing mice received US irradiation. Serum was collected. Using CD11c, CD86, CD80 monoclonal antibody staining and flow cytometry detection.

In Vivo CT26 Orthotopic and Bilateral Tumor Model. The experiment selected 7-week-old female BALB/c mice. Firstly, one million CT26 cells were subcutaneously injected into the right side of each mouse, and after one week, half of one million CT26 cells were injected into the left side of the mouse. Then, these mice were randomly divided into 6 groups (7 in each group): (1) PBS, (2) BCO, (3) BCO-V_{Cu}, (4) PBS + US irradiation, (5) BCO + US irradiation, and (6) BCO-V_{Cu} + US irradiation. At 8 h after the injection of material into the tail vein of mice, the mice were exposed to US irradiation. Measure body weight and tumor size every 3 days. The volume of primary and distant tumors is determined by the formula $V = \text{length} \times \text{width} \times \text{high}^2/2$.

RNA Sequencing Methods for Transcriptome Analysis. Total RNA was extracted from tumor tissues using the TRIzol reagent. The purified RNA was reverse-transcribed to create complementary DNA (RNeasy Micro Kit, QIAGEN, Valencia, CA, USA). Each experiment was performed in triplicate, and RNA sequencing was performed using Metware Technology (Wuhan, China).

Statistical Analysis. All experiments with BCO-V_{Cu} were repeated at least three times. All *in vivo* experiments were conducted after randomization, and at least five mice were applied in one group in the animal experiments. The statistical analysis was performed using GraphPad Prism 8.0 software. All the results were presented as mean \pm SD. n.s. represented no significance, asterisks were applied to represent significant differences (* $p < 0.05$, ** $p < 0.01$, *** $p < 0.001$, and **** $p < 0.0001$).

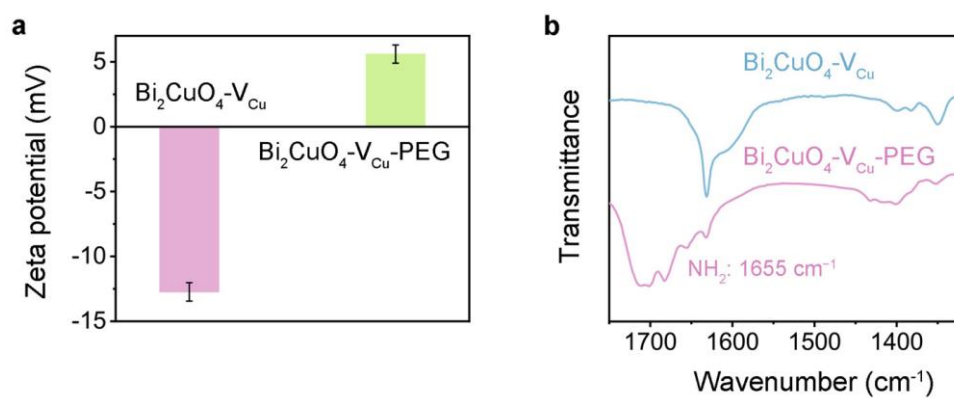


Figure S1. (a) Zeta potentials of $\text{Bi}_2\text{CuO}_4\text{-V}_{\text{Cu}}$ and $\text{Bi}_2\text{CuO}_4\text{-V}_{\text{Cu}}\text{-PEG}$. (b) FTIR spectra of the samples.

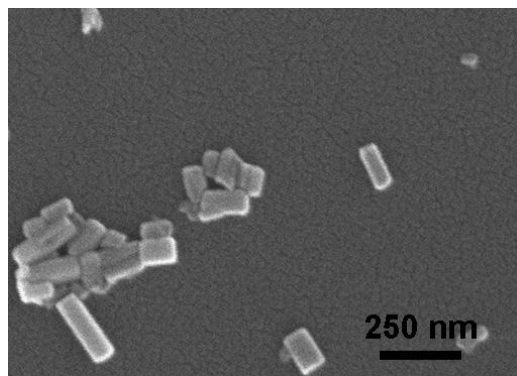


Figure S2. SEM image of BCO-V_{cu}.

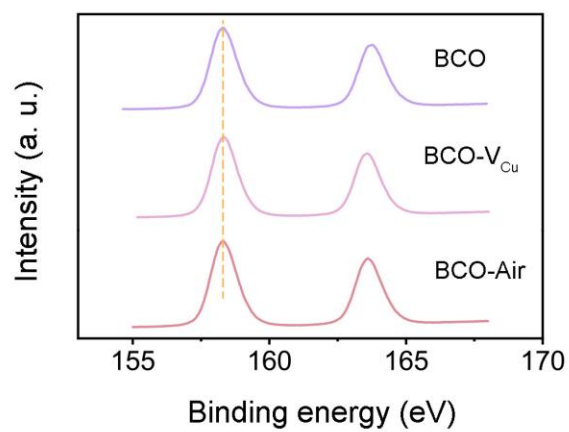


Figure S3. XPS spectra of Bi 4f.

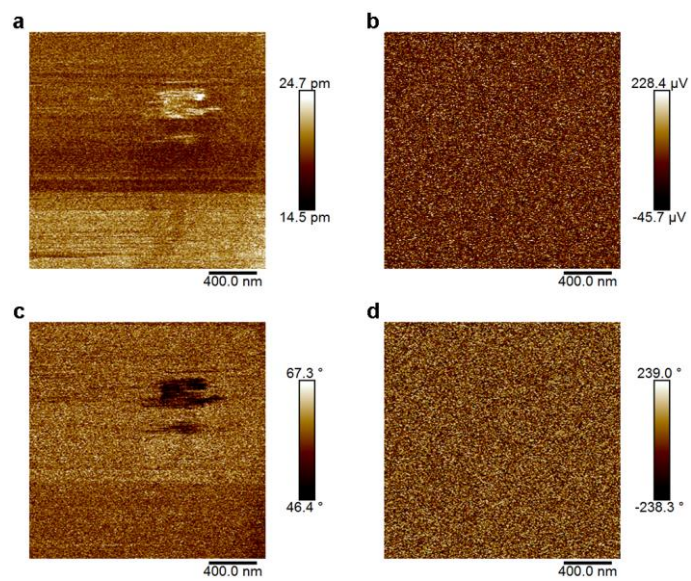


Figure S4. (a) Out-of-plane and (b) in-plane PFM amplitude images of BCO-V_{Cu}. (c) Out-of-plane and (d) in-plane PFM phase images.

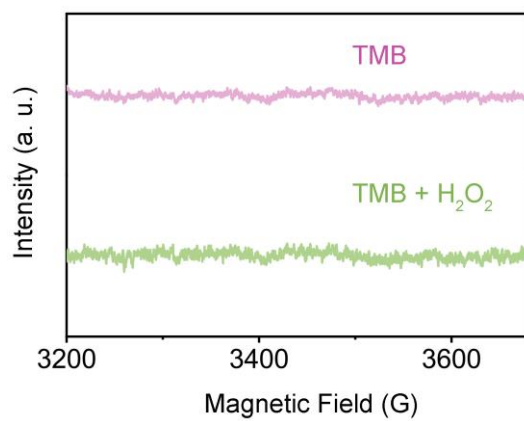


Figure S5. ESR spectra of different groups used for the detection of $\cdot\text{OH}$.

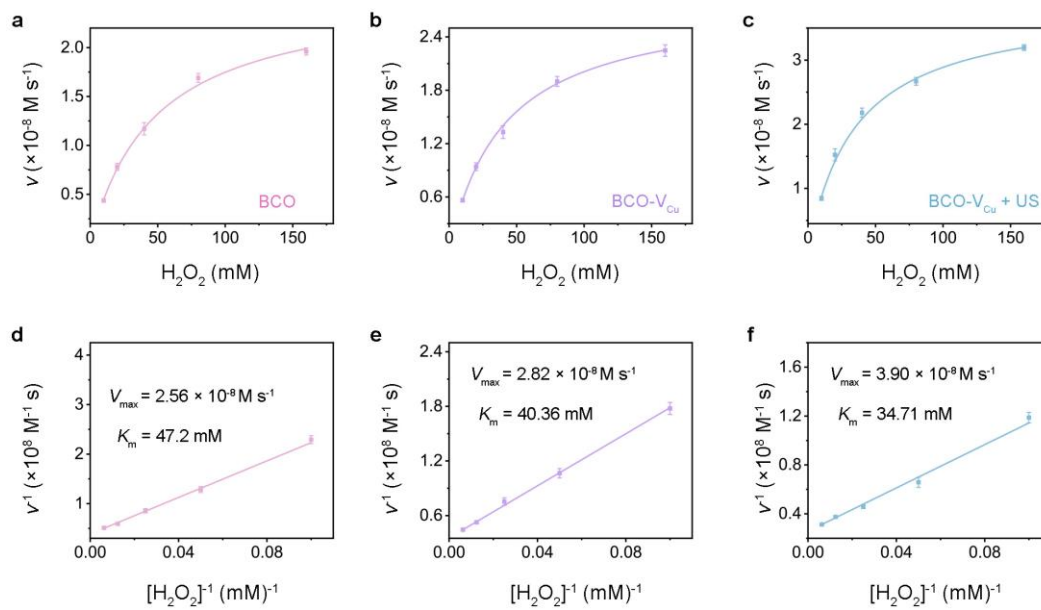


Figure S6. The corresponding (a–c) steady-state kinetic assay analysis and (d–f) Lineweaver–Burk plotting.

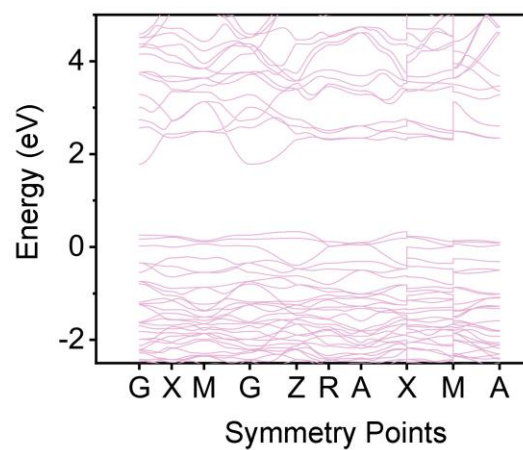


Figure S7. The DFT + U electronic band structures of BCO.

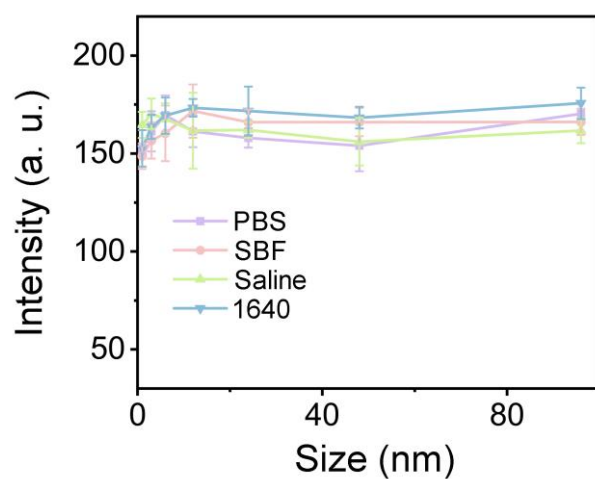


Figure S8. Dynamic light scattering (DLS) size distribution profiles of BCO- V_{Cu} in different media. Data are expressed as mean \pm S.D. ($n = 3$)

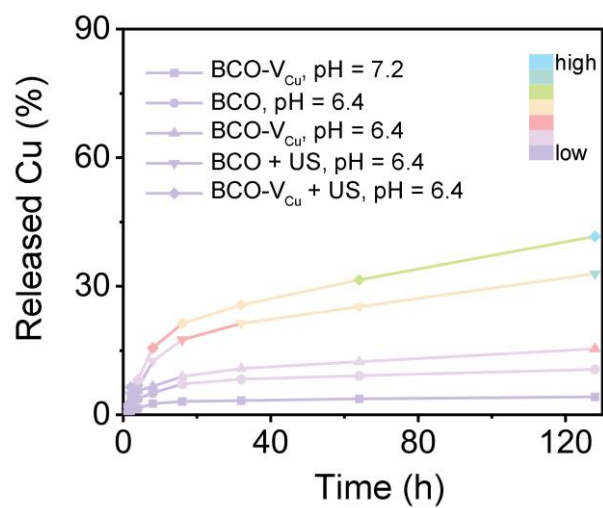


Figure S9. Accumulated releasing Cu from different conditions.

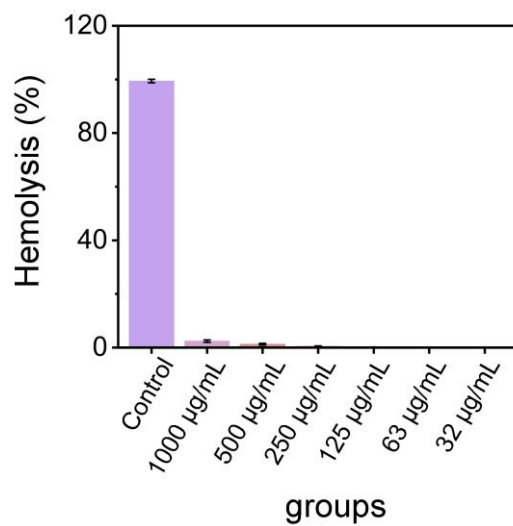


Figure S10. *In vitro* toxicity experiments results. The Hemolysis test of the as-prepared BCO-V_{Cu} (32, 63, 125, 250, 500, 1000 µg/mL dispersed in PBS solution).

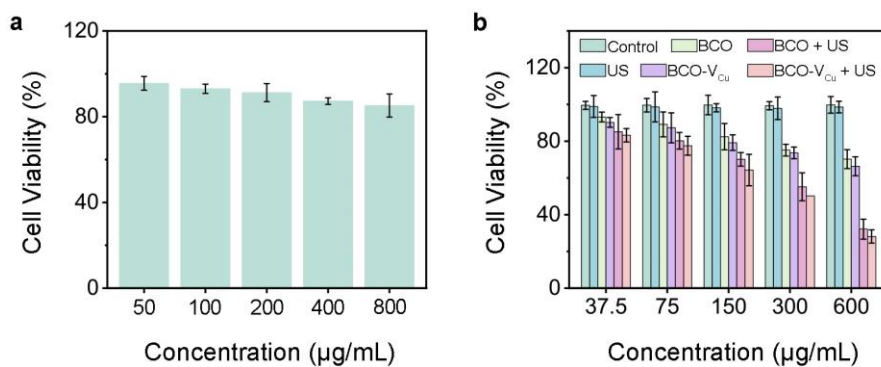


Figure S11. (a) Cell viability of L929 cells incubated with BCO- V_{Cu} at different concentrations for 24 h. (b) Cell cytotoxicity of CT26 cells under different conditions ($n = 3$, mean \pm SD).

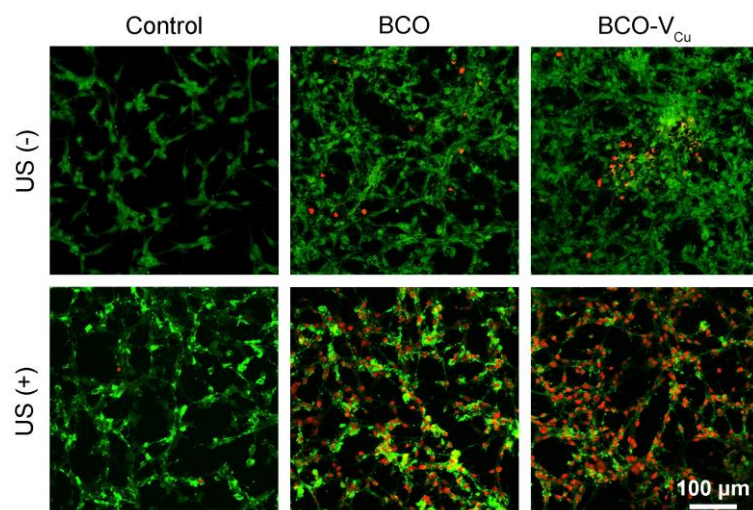


Figure S12. Calcein-AM/PI double staining of CT26 cells after different treatments.

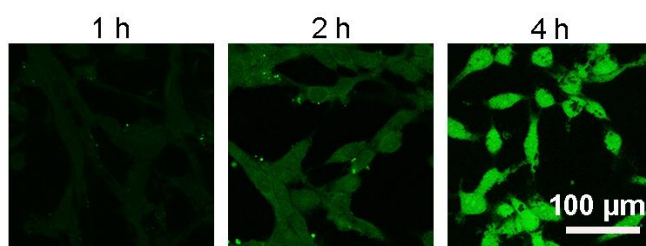


Figure S13. CLSM mages of CT26 cells incubated with BCO-V_{Cu} at various time intervals.

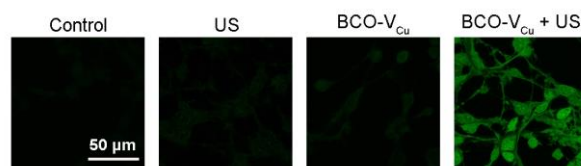


Figure S14. Confocal microscopy images of cells with various treatments of intracellular Ca^{2+} stained with Fluo-4 AM.

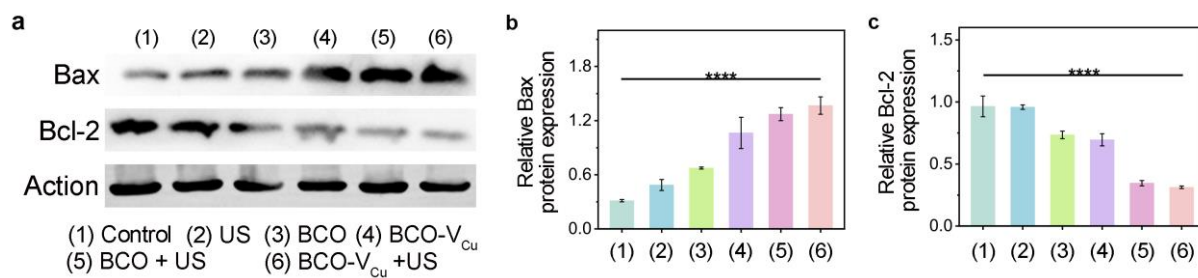


Figure S15. (a) Measurement of Bax and Bcl-2 expression by western blot in CT26 cells cultured with different treatments. Western Blotting detection of (b) Bax and (c) Bcl-2 expression levels of tumor sections. Data presented as mean \pm S.D. (n = 3). n.s. represented no significance, * $p < 0.05$, ** $p < 0.01$, *** $p < 0.001$, **** $p < 0.0001$.

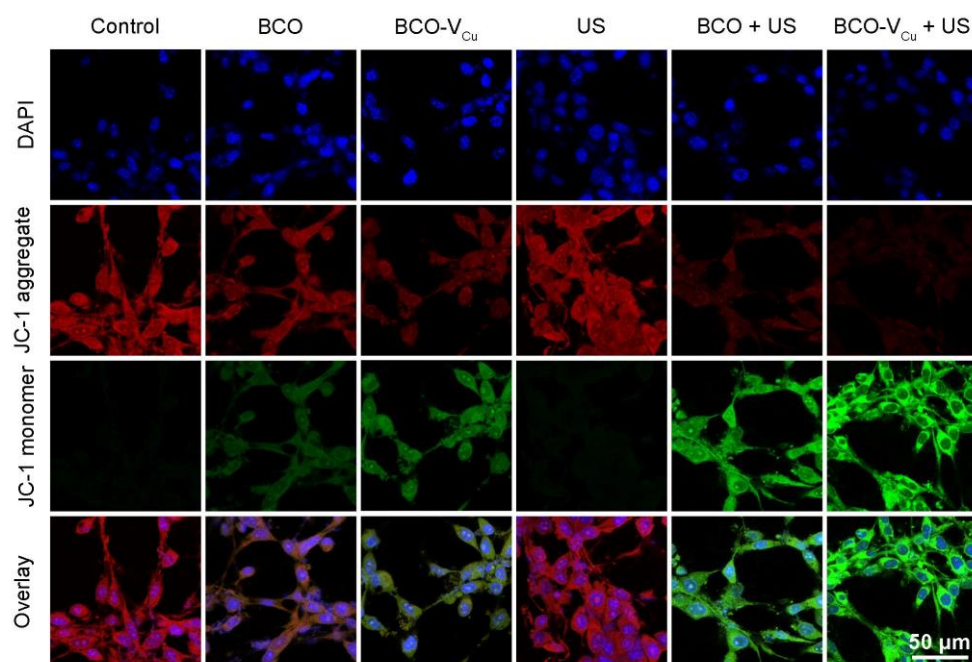


Figure S16. JC-1 staining of CT26 cells after different treatments. The red JC-1 aggregates mean mitochondria with a normal membrane potential, and the green JC-1 monomer indicates the mitochondria with a depolarized membrane.

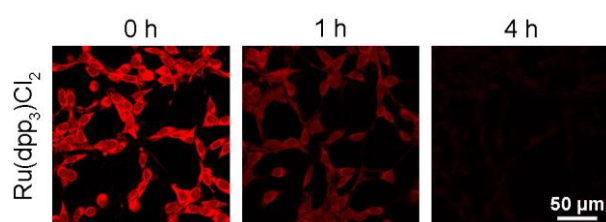


Figure S17. Intracellular O_2 generation using $[\text{Ru}(\text{dpp})_3]^{2+}\text{Cl}_2$ as a probe.

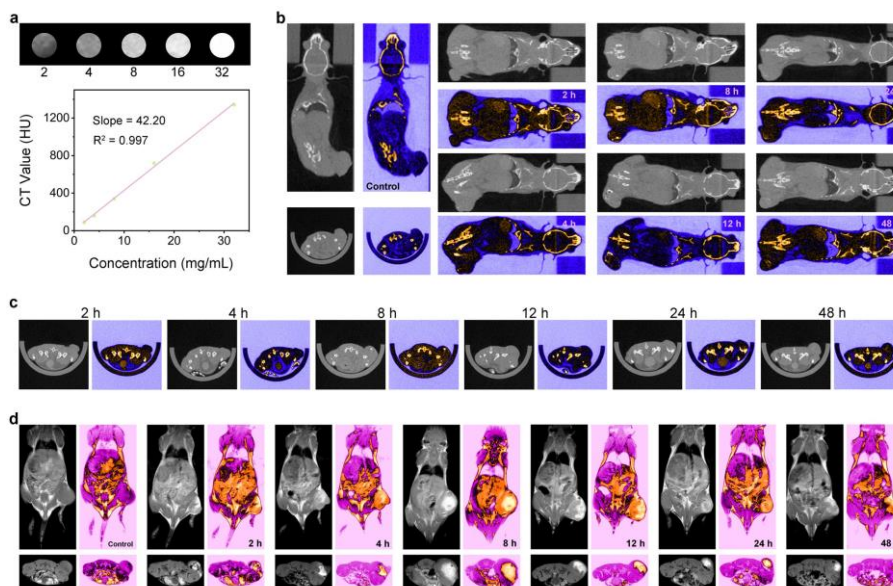


Figure S18. *In vitro* and *in vivo* CT and MR Imaging. (a) *In vitro* CT images of BCO- V_{Cu} with different concentrations and CT values. *In vivo* (b) coronal and (c) transverse sections of tumor region of tumor-bearing mice after i.v. injection of BCO- V_{Cu} at different time intervals. (d) MR imaging of mice at various time intervals injection BCO- V_{Cu} .

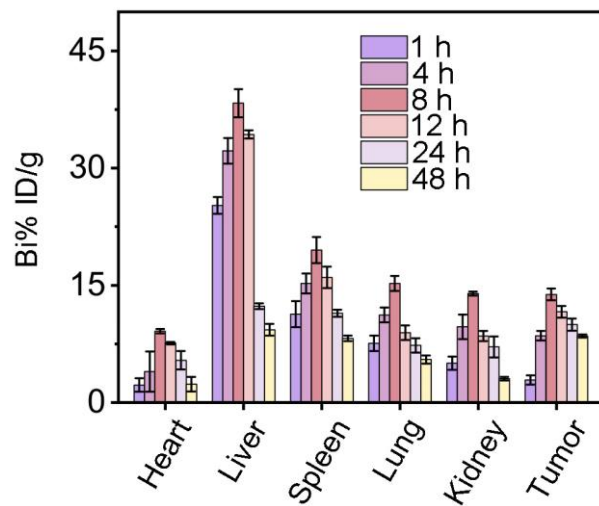


Figure S19. Biodistribution of Bi in tumor and main organs after injection with BCO-V_{Cu} intravenously for different times.

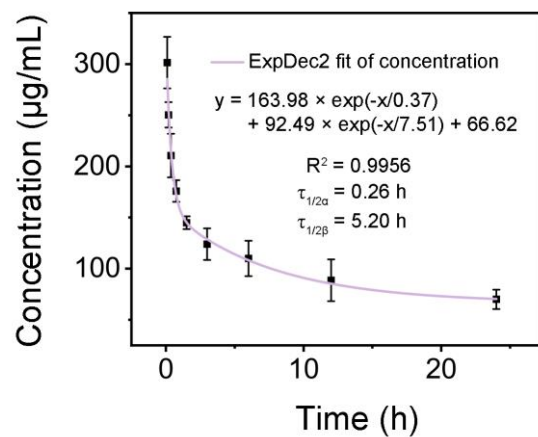


Figure S20. Blood circulation curve of intravenously injected BCO- V_{Cu} . Data are expressed as mean \pm S.D. ($n = 3$).

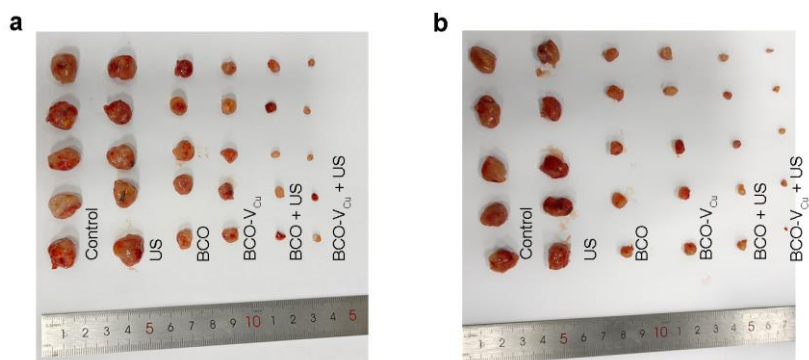


Figure S21. Photos of excised (a) primary and (b) distant tumor tissues from different groups of mice at the end of treatment.

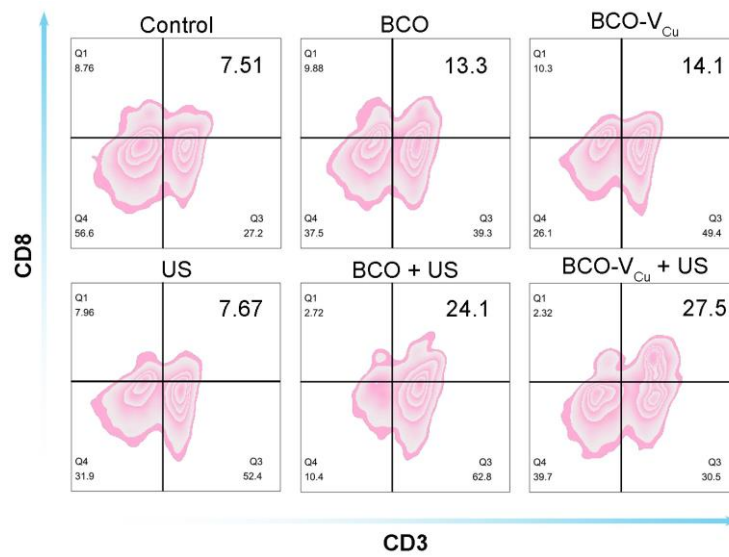


Figure S22. FCM analysis of the percentages of CD8⁺ T cells in spleens of mice after different treatments.

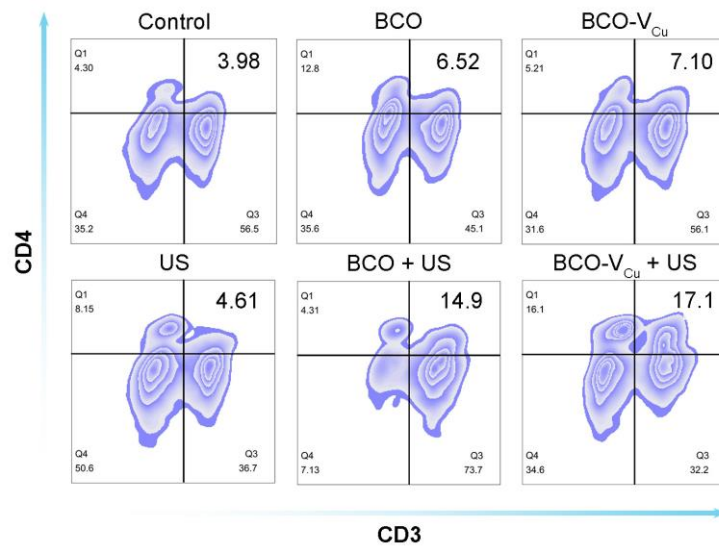


Figure S23. FCM analysis of the percentages of CD4⁺ T cells in spleens of mice after different treatments.

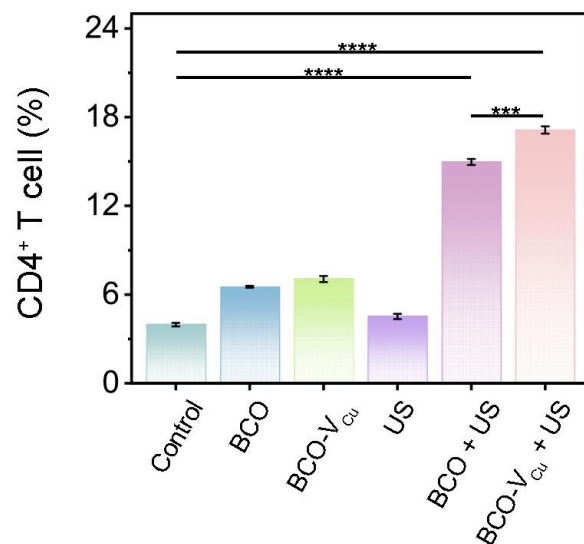


Figure S24. Spleen investigation. Proportions of CD4⁺ T cells in spleen tissues. Data presented as mean \pm S.D. (n = 3). n.s. represented no significance, * $p < 0.05$, ** $p < 0.01$, *** $p < 0.001$, **** $p < 0.0001$.

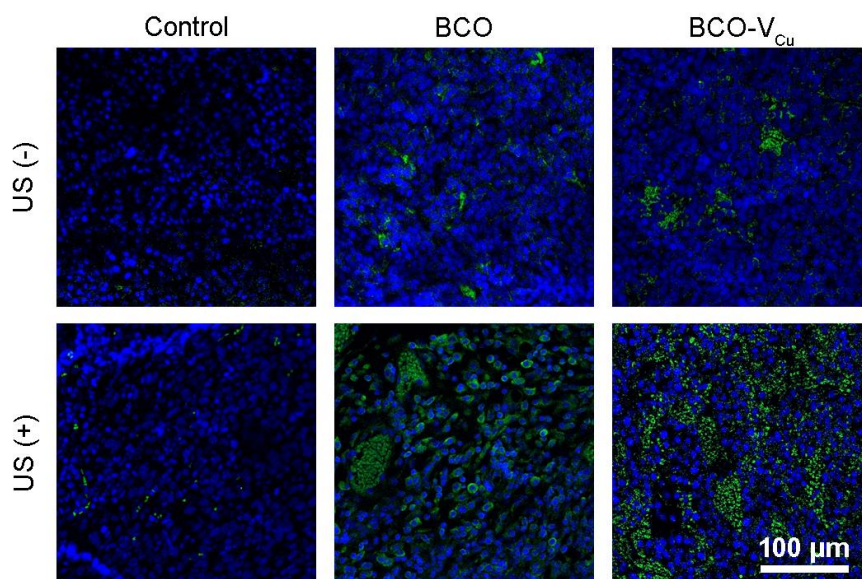


Figure S25. Immunofluorescence images of nuclear staining (blue) and anti-iNOS antibody staining (green) in distant tumor sections.

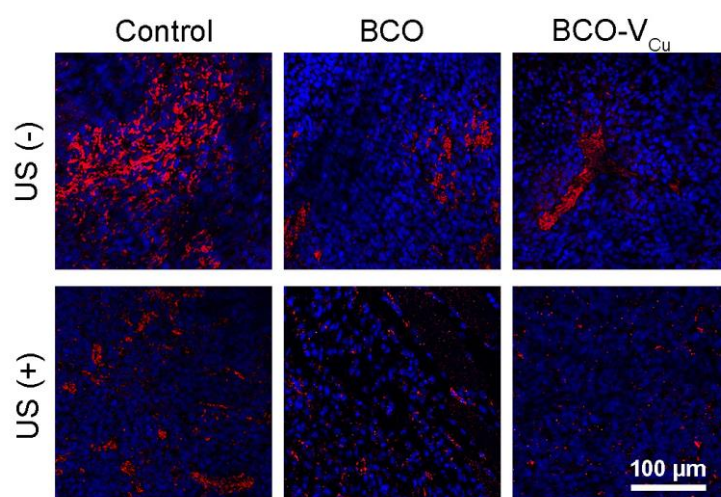


Figure S26. Immunofluorescence images of nuclear staining (blue) and anti-CD206 antibody staining (red) in distant tumor sections.

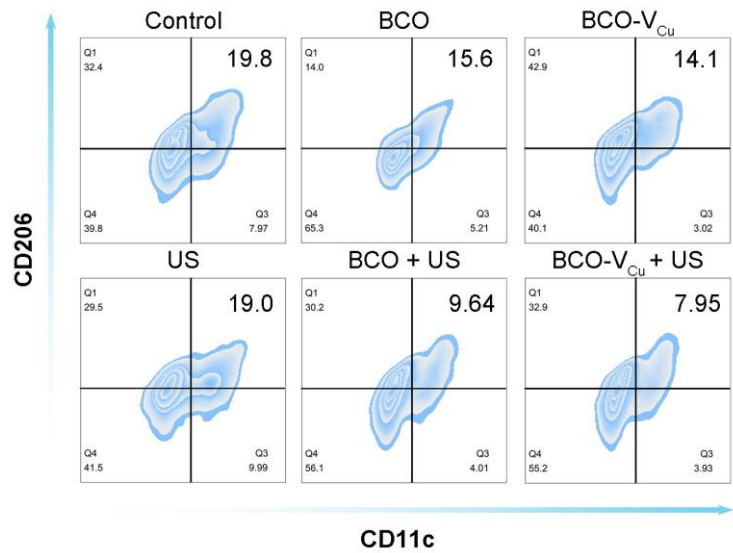


Figure S27. FCM analyses of the percentages of M2 TAMs in primary tumor of mice after different treatments.

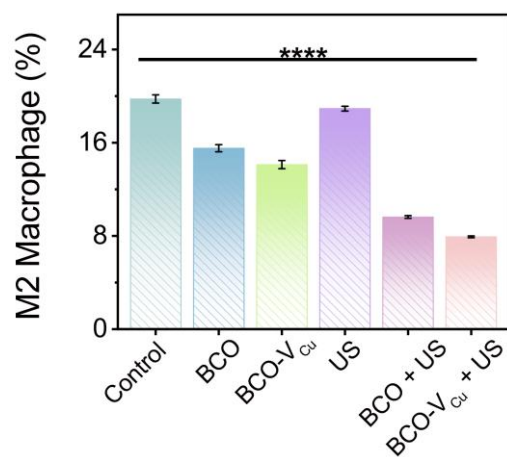


Figure S28. Statistical analysis of maturation rates of M2 macrophages.

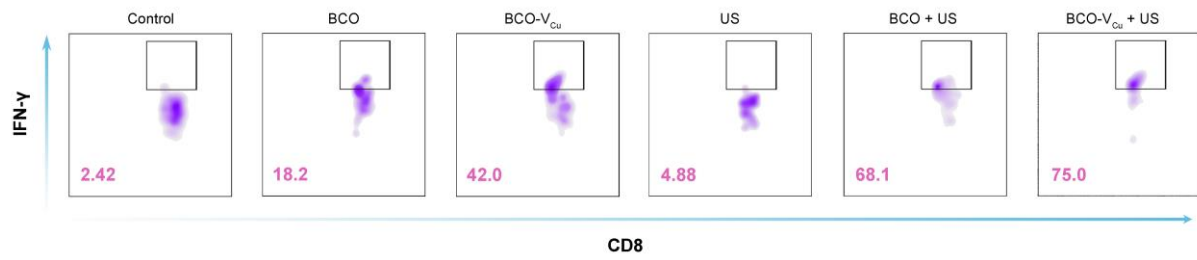


Figure S29. Flow cytometry detection of IFN- γ ⁺ CD8⁺ T cells.

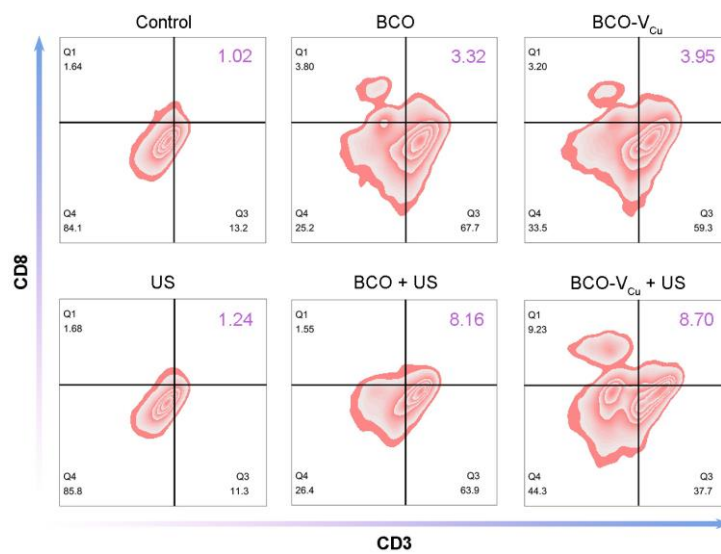


Figure S30. FCM analyses of the percentages of CD8⁺ T cells in primary tumor of mice after different treatments.

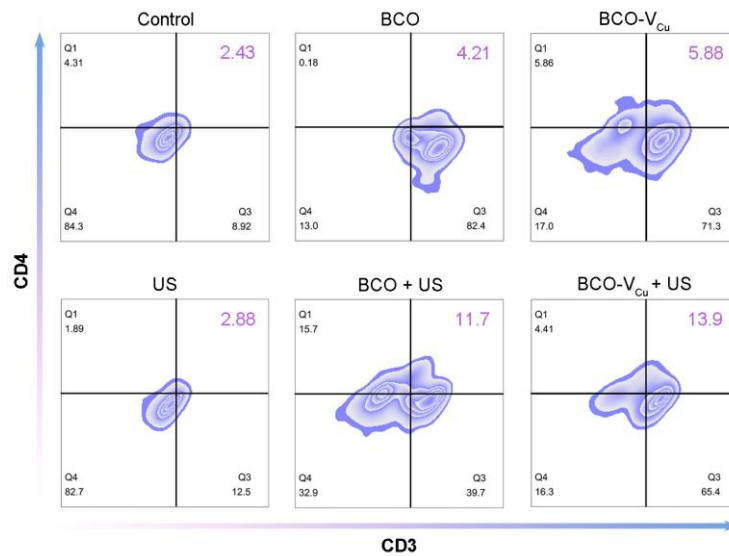


Figure S31. FCM analyses of the percentages of CD4⁺ T cells in primary tumor of mice after different treatments.

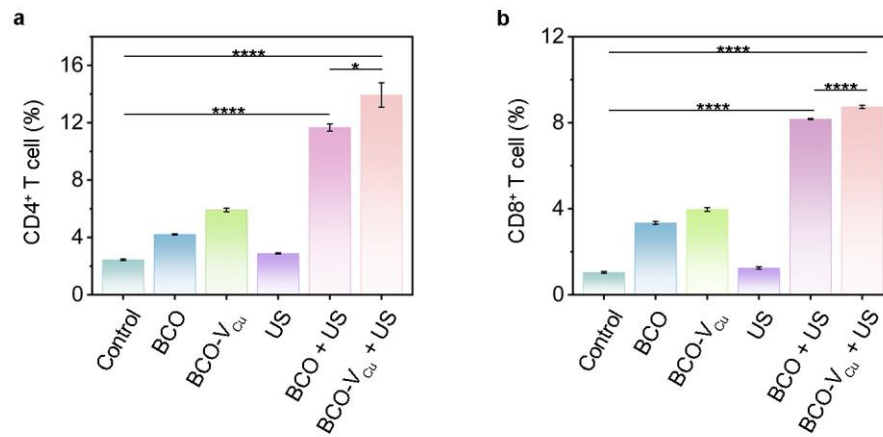


Figure S32. (a) Primary tumor investigation. Proportions of CD4⁺ T cells in tumor tissues. (b) Primary tumor investigation. Proportions of CD8⁺ T cells in tumor tissues. Data presented as mean \pm S.D. (n = 3). n.s. represented no significance, * $p < 0.05$, ** $p < 0.01$, *** $p < 0.001$, **** $p < 0.0001$.

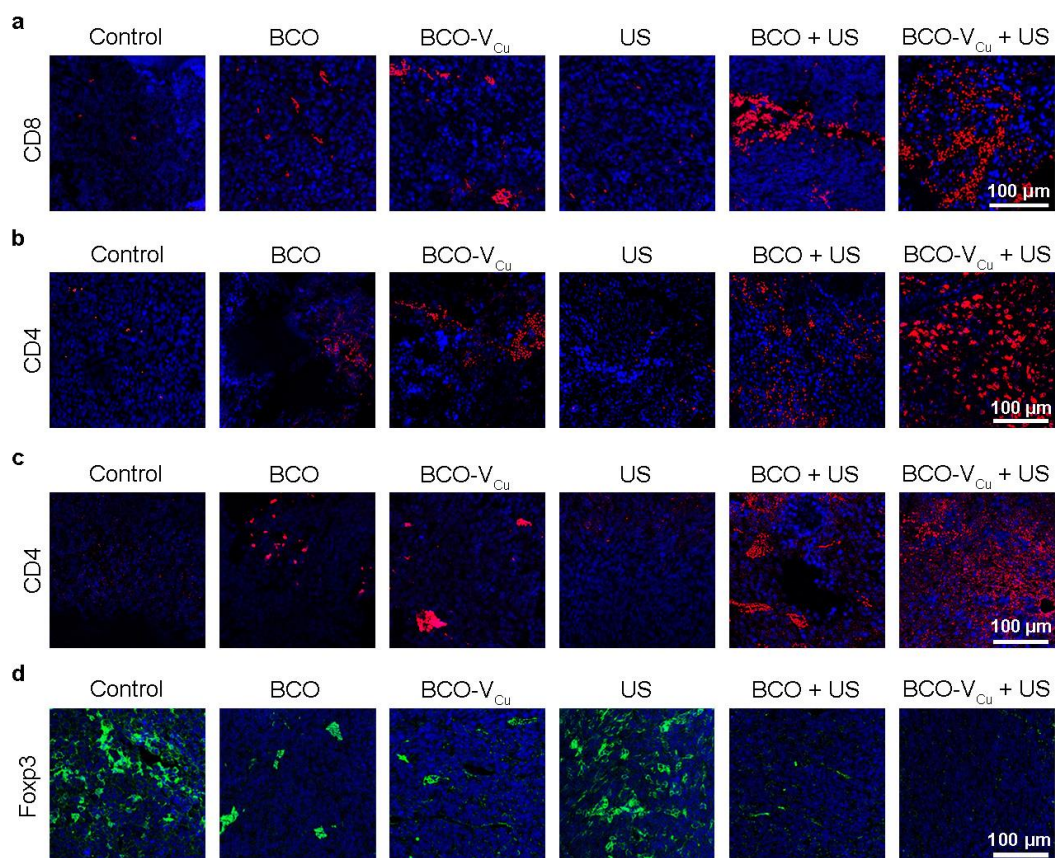


Figure S33. (a) Immunofluorescence images of nuclear staining (blue) and anti-CD8 antibody staining (red) in distant tumor sections. (b) Immunofluorescence images of nuclear staining (blue) and anti-CD4 antibody staining (red) in primary tumor sections. (c) Immunofluorescence images of nuclear staining (blue) and anti-CD4 antibody staining (red) in distant tumor sections. (d) Immunofluorescence images of nuclear staining (blue) and anti-Foxp3 antibody staining (green) in primary tumor sections.

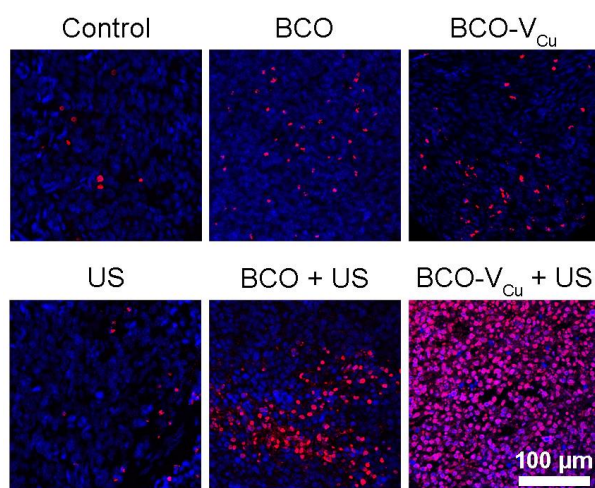


Figure S34. TUNEL staining of primary tumor sections from CT26 cells tumor-bearing mice on the 21st day of treatment.

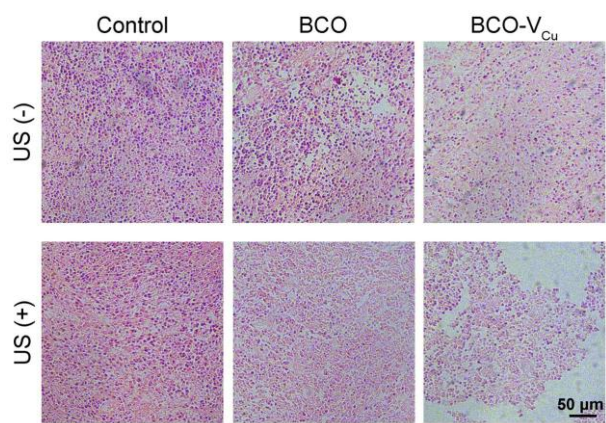


Figure S35. H&E staining images of tumor after treatments.

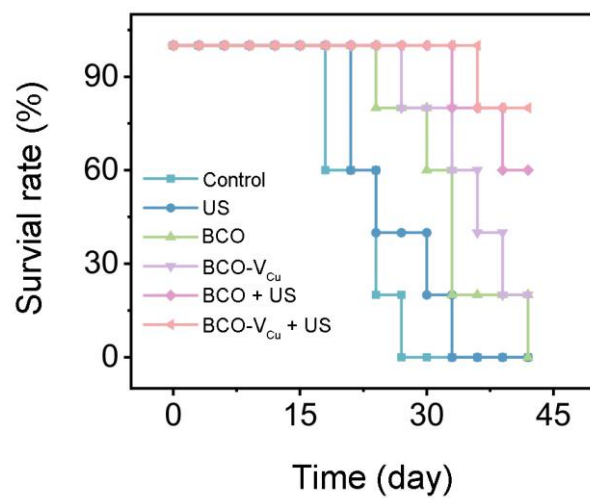


Figure S36. Survival percentage of tumor-bearing nude mice after different treatments (n = 5).

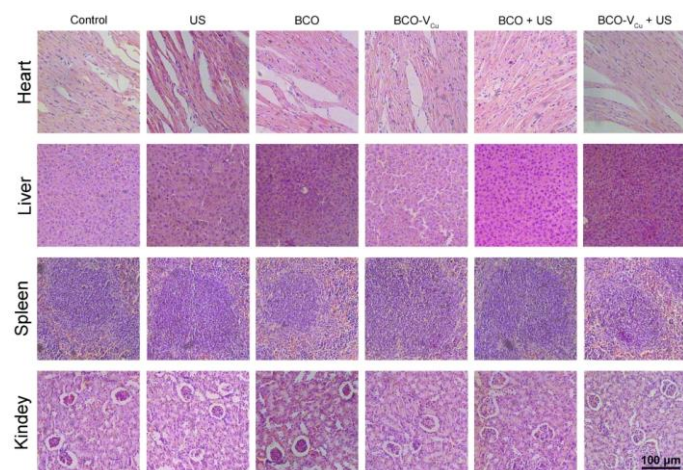


Figure S37. H&E staining images of major organs after treatments.

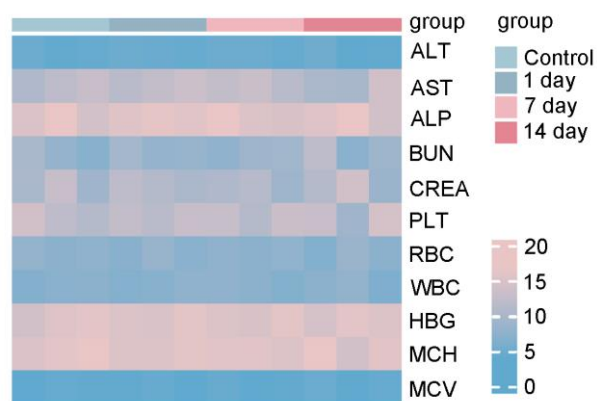


Figure S38. The blood biochemistry and hematological test results following BCO- V_{Cu} + US treatment in mice at various time points. The blood biochemistry includes the liver function indicators alanine aminotransferase (ALT), alkaline phosphatase (ALP), aspartate aminotransferase (AST), blood urea nitrogen (BUN) and blood creatinine (CREA). Complete blood count including: platelets (PLT), red blood cells (RBC), white blood cells (WBC), hemoglobin (HGB), mean corpuscular hemoglobin (MCH) and mean corpuscular volume (MCV).

Table S1. Comparison of Cu^{2+} , Cu^+ and their ratio obtained from high-resolution Cu 2p XPS spectra. The ratio is calculated based on the integrated area of Cu^{1+} and Cu^{2+} peaks.

Sample	The area% of Cu^{2+}	The area% of Cu^+	The ratio of $\text{Cu}^+ / (\text{Cu}^+ + \text{Cu}^{2+})$
BCO	61.67	8.95	0.127
BCO-Air	58.57	17.35	0.229
BCO- V_{Cu}	53.73	18.93	0.261